

Learned Single-Pass Multitasking Perceptual Graphics for Immersive Displays

DOĞA YILMAZ, Özyeğin University, Türkiye

TOWAKI TAKIKAWA, University of Toronto, Canada

DUYGU CEYLAN, Adobe Research, United Kingdom

KAAN AKŞIT, University College London, United Kingdom

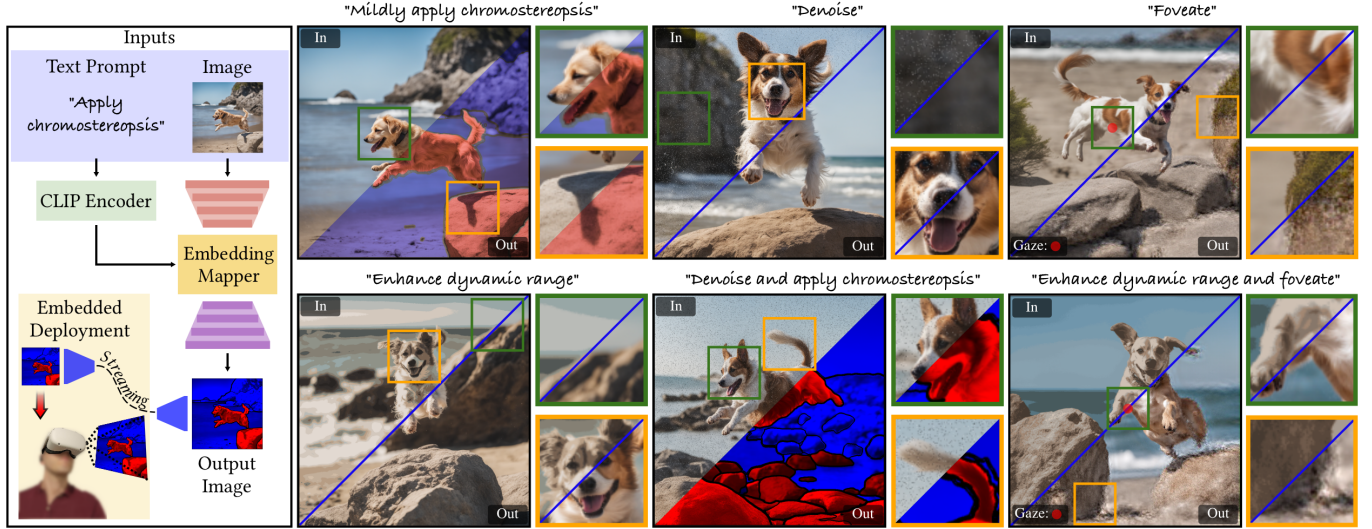


Fig. 1. Learned Multitasking Perceptual Graphics for Immersive Displays is a novel text-guided model (left) that perceptually enhances input images based on given prompts. This new model (right) supports various perceptual graphics methods including Chromostereopsis, Denoising, Foveation, and Dynamic Range modification, and their permutations at different intensities using adjectives like “mildly”, “slightly”, and “lightly” within a single inference process, eliminating the need for daisy-chaining multiple models. Source images are generated using Stable Diffusion [34].

Immersive displays are advancing rapidly in terms of delivering perceptually realistic images by utilizing emerging perceptual graphics methods such as foveated rendering. In practice, multiple such methods need to be performed sequentially for enhanced perceived quality. However, the limited power and computational resources of the devices that drive immersive displays make it challenging to deploy multiple perceptual models simultaneously.

We address this challenge by proposing a computationally-lightweight, text-guided, learned multitasking perceptual graphics model. Given RGB input images, our model outputs perceptually enhanced images by performing one or more perceptual tasks described by the provided text prompts. Our model supports a variety of perceptual tasks, including foveated rendering, dynamic range enhancement, image denoising, and chromostereopsis, through multitask learning. Uniquely, a single inference step of our model supports different permutations of these perceptual tasks at different prompted rates (i.e. mildly, lightly), eliminating the need for daisy-chaining multiple models to get the desired perceptual effect. We train our model on our new dataset of source and perceptually enhanced images, and their corresponding text prompts. We evaluate our model’s performance on embedded platforms and validate the perceptual quality of our model through a user study. Our method achieves on-par quality with the state-of-the-art task-specific methods using a single inference step, while offering faster inference speeds and flexibility to blend effects at various intensities.

CCS Concepts: • **Computing methodologies** → **Perception; Mixed / augmented reality; Neural networks.**

Additional Key Words and Phrases: Perceptual Graphics, Virtual Reality, Augmented Reality, Immersive Displays

1 INTRODUCTION

Immersive display technologies [23], including Augmented Reality (AR) glasses, Virtual Reality (VR) headsets, and large-format displays, are advancing towards more realistic image delivery. However, these devices face constraints due to power, performance, and form-factor limitations, making on-device high-quality rendering a challenge. Hence, researchers explore perceptual graphics methods such as foveated rendering [37], dynamic range enhancement [27], image denoising [9], and chromostereopsis [40] to enhance low quality images. In practice, these emerging perceptual graphics methods need to be daisy-chained to produce images of high perceptual quality. However, daisy-chaining these perceptual models can quickly exhaust computational resources. A potentially more resource-efficient alternative to daisy-chaining is to combine multiple perceptual graphics methods with a multitask learning approach. Recent works in generative models have demonstrated that combined learned multimodal approaches, enables a wide range of

image-to-image translation tasks [15, 34]. Inspired by these recent works, we propose to unify perceptual tasks in a single model to utilize the power, bandwidth, and computational resources more efficiently.

Our work proposes a text-guided learned multitasking perceptual graphics model for immersive displays. The input to this model is an RGB image and text prompt pair to guide the model to output perceptually enhanced images. Our model is enabled by our new learned component that efficiently combines encoded RGB images and embeddings from text prompts at the bottleneck of a multitasking U-Net. Leveraging multitask learning, our model supports various perceptual tasks and their combinations, including foveated rendering, dynamic range enhancement, image denoising, and chromostereopsis.

To train our model, we introduce a new dataset comprising pairs of images and their text prompts, each representing a distinct perceptual effect. This model facilitates deployment on both desktop and embedded systems for immersive displays as it is lightweight and fast. Furthermore, we validate the perceptual quality of the images generated by our model with a subjective experiment. Our contributions are as follows:

- *Multitasking Perceptual Model.* Enabled by our new learned embedding mapper, which efficiently combines image and text embeddings, we propose a learned multitasking perceptual graphics model that transforms RGB images to various perceptually guided image styles. Our model can achieve hybrid tasks that are composed of permutations of individual tasks (e.g., enhance dynamic range and foveate) as well as controlling the degree of applied effect (e.g., mildly apply chromostereopsis) in a single inference step. Furthermore, we deploy our model on embedded devices (i.e., Nvidia Jetson Nano) to demonstrate its effectiveness in computationally limited scenarios.
- *Perceptual Evaluations.* We introduce a new dataset that contains pairs of images. Each pair represents an image-to-image translation of perceptual effects. We also provide a complete pipeline describing the image generation routine in our datasets. Utilizing this dataset and image generation pipelines, we validate the perceptual quality of the generated images from our multitasking perceptual model through a tailored user study.

The source code of our learned model, along with our perceptual image dataset and model weights, can be found at [REVIEW].

2 RELATED WORK

Our work enables the simultaneous application of multiple perceptual graphics tasks to efficiently prepare media for immersive displays by leveraging multitask learning. We review the relevant literature for each visual perception task we focus on, as well as for learned image processing methods and multitask learning approaches, to provide context for our contributions.

2.1 Visual Perception Tasks

Our work focuses on foveation, dynamic range enhancement, image denoising, and chromostereopsis. Image denoising and dynamic range enhancement are well established tasks in the literature, whereas foveation and chromostereopsis tasks are actively being

Table 1. Overview of perceptual graphics techniques. Our work distinguishes itself by providing support for multiple perceptual effects in a single inference pass. Our model is also text-guided and multitasking, while maintaining a lightweight architecture. For the supported perceptual tasks, we use the following abbreviations: Foveation (F), Chromostereopsis (C), Image Denoising (ID), and Dynamic Range Enhancement (DRE).

	Approach	Perceptual Tasks	Text Guidance	Speed	Multitasking
Walton et al. [39]	Traditional	F	None	Offline	None
Deza et al. [10]	Learned	F	None	Real Time	None
Westermann et al. [40]	Traditional	C	None	Real Time	None
Conde et al. [9]	Learned	ID	None	Real Time	None
Marzuki et al. [27]	Learned	DRE	None	Real Time	None
Afifi et al. [1]	Learned	None	None	Real Time	Shared Encoder
Sun et al. [35]	Learned	None	Fixed Wording	Real Time	Hard Parameter Sharing
Huang et al. [15]	Learned	None	Open Ended	Offline	Hard Parameter Sharing
Ours	Learned	F, C, ID, DRE	Semi-Open Ended	Real Time	Hard Parameter Sharing

explored. Here, we refer dynamic range enhancement as increasing the bits used to represent brightness levels in an image. Following the common literature in image denoising [9, 29, 44] and dynamic range enhancement [6, 27, 43], we train our model using pairs of images with low and high dynamic range and image pairs containing noisy and noise-free images, respectively. We provide an overview of existing perceptual graphics techniques in Tbl. 1.

Foveation. Foveated rendering promises to reduce computational complexity by rendering perceptually accurate yet lower resolution images in the periphery, leveraging the variation in resolution acuity between the fovea and periphery in the Human Visual System (HVS). Meng et al. [28] parameterizes foveated rendering by embedding polynomial kernel functions in the classic log-polar mapping, enabling variation in the sampling density and distribution of the rendered images. Another class of methods for foveated rendering uses metamers [10, 37, 39], which are image patches that are perceptually indistinguishable despite being different in terms of pixel values. Display hardware devices have recently adopted designs specifically catered towards foveated rendering [20], especially for AR and VR applications. *Our model follows the metamer approach proposed by Walton et al. [39] to foveate images.*

Chromostereopsis. Chromostereopsis [2, 30, 40] is a visual perceptual effect induced by using different colors in images, which leads to an illusion of perceived depth differences in various colors of the images. Hong et al. [14] propose an algorithm to enhance perceived depth in images based on chromostereopsis and cubic effects. Similarly, Jung et al. [17] introduce a depth map-based image enhancement algorithm utilizing chromostereopsis. Westermann et al. [40] recently proposed a novel rule-based method to enhance perceived depth in images, using results from a user study. *Building on Westermann et al. [40], our work focuses on creating artistically appealing chromostereoptic images that maximize perceived depth.*

2.2 Learned Multitasking Image Processing

We employ a learning-based pipeline and, to provide context for our contributions, we review existing learned image-to-image translation methods and multitask learning approaches.

Learned image-to-image translation. Isola et al. [16] investigate conditional Generative Adversarial Network (GAN) as a general-purpose solution for image-to-image translation tasks. Zhu et al. [46] propose an unpaired image-to-image translation method using a cycle-consistent approach, which mitigates the need for paired training data. Additionally, Choi et al. [7] propose a novel approach for multidomain image-to-image translations using a single model. Recently, Ko et al. [22] introduce an independent classifier to enhance feature learning, addressing the limitations of Choi et al.’s method [7]. Ke et al. [19] propose a memory efficient neural color mapping for color normalization and stylization. Text-guided diffusion-based generative models have also been utilized for image-to-image translation [3, 15]. However, these generative models are iterative and rely on large pretrained models, requiring significant computational power, making their deployment in computationally limited scenarios challenging. We have examined the methods proposed by Ke et al. [19] and Brooks et al. [3] in our context, finding them unsuitable for our application primarily due to excessive computational demands and low image quality with noticeable artifacts for our perceptual tasks. Detailed results from these investigations are presented in the supplementary’s Sec. 1. *Our work stands out as a lightweight application-specific solution suitable for embedded deployment, offering a text-guided tailored approach to applying perceptual graphics tasks for immersive displays.*

Multitask learning. Introduced by Caruana [4], Multitask Learning (MTL) is an inductive transfer mechanism aimed at improving generalization performance by leveraging the domain-specific information contained in the training signals of related tasks. In our work, we focus on hard parameter sharing, where all tasks share the same network architecture and parameters. The work by Sun et al. [36] propose an efficient sharing scheme that learns separate execution paths for different tasks. In addition, Afifi et al. [1] propose a deep multitask learning architecture for auto white balancing, utilizing a single encoder and multiple decoders, each corresponding to a specific task. Following up Afifi et al. [1], Sun et al. [35] demonstrate multitasking with a single task-conditioned decoder. Alternatively, diffusion-based generative models could be utilized in multitask learning scenarios [15], but not suitable for embedded development. *Similar to the architecture proposed by Sun et al. [35], our work utilizes task embeddings to learn multiple tasks with hard parameter sharing in the encoder and decoder. Our main difference is in how we combine image and text embeddings. In particular, we propose an efficient embedding mapper module that only acts at the bottleneck of our model.*

The aforementioned perceptual tasks and learned perceptual methods have been well explored individually. Yet, the unification of these tasks into a single model remains an open challenge. *Uniquely, our solution offers a text-guided multitasking model capable of applying all these perceptual tasks within a single, fast, cohesive model that can be deployed in embedded scenarios.*

3 TEXT-GUIDED PERCEPTUAL GRAPHICS

Given an input RGB image and a text prompt describing the desired perceptual effect, our model, as depicted in Fig. 2, applies the effect such as foveation, dynamic range enhancement, image denoising,

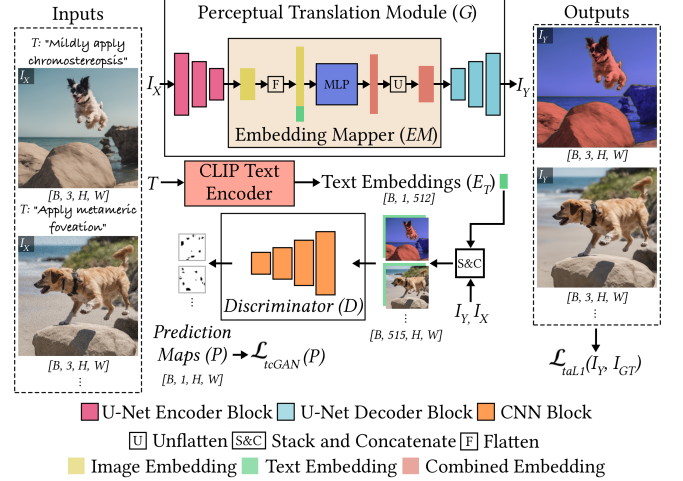


Fig. 2. Our proposed text-guided perceptual graphics model. Perceptual translation component (G) is conditioned on text embeddings (E_T) generated using a pre-trained CLIP Text Encoder (CLIP) [32] and an Embedding Mapper module (EM). Embedding mapper module (EM) is a Multilayer Perceptron (MLP) that concatenates the text embeddings (E_T) and image embeddings (E_I) to generate a combined embedding (E_C). The task-aware discriminator (D) evaluates the generated image (I_Y) based on the task-specific text embedding (E_T) and input image (I_X) for regularization purposes.

and chromostereopsis, as well as their permutations at intended scales (i.e. “mildly,” “lightly”).

Our model comprises two main components: a perceptual translation component, G, and a task-aware discriminator component, D. Firstly, our perceptual translation component, G, a modified U-Net, transforms input images into perceptually enhanced output images. This component incorporates an embedding mapper module, EM, which conditions the perceptual translation based on embeddings derived from the provided input text prompts. Secondly, our discriminator, D, guides the training of perceptual translation component, G, by verifying the outputs according to the task embeddings. At test time, D is not deployed for computational efficiency, as it is only used for training G. Additionally, for extreme cases such as scenarios with very low bandwidth and low power, we utilize a pre-trained autoencoder [34] to stream the generated images in a compressed format to the user, ensuring high-quality presentation of media.

Our model is trained using a sample size adaptive loss function, which scales the loss based on the number of samples available for each task and a task-aware adversarial loss, which evaluates the generated images based on the task-specific text embeddings. To train and evaluate our model, we introduce a dataset comprising pairs of images, each representing a distinct image-to-image translation effect based on various perceptual enhancements.

Perceptual image translation component. Our first component, the perceptual image translation component G, has two primary objectives: (1) to enhance the visual perception of input images with

desired effects, and (2) to ensure the model is lightweight and suitable for edge devices. To meet all these requirements, we employ a U-Net architecture, similar to [16], with a modified bottleneck layer, and a pre-trained CLIP model [32] for text prompt guidance. First, we transform the input text prompts, T , into text embeddings, E_T , using the pre-trained CLIP model, $CLIP$. In parallel, we encode the input images, I_X , into image embeddings, E_I , using the encoder of the U-Net. Following this, we flatten the text embeddings, E_T , and image embeddings, E_I , and concatenate them to form a single embedding, E_{T+I} . This concatenated embedding, E_{T+I} , is then fed into our embedding mapper module, EM . EM module, which consists of a MLP, maps the concatenated embedding, E_{T+I} , to generate a combined embedding, E_C . This operation not only merges text and image information into a single embedding but also ensures that the dimensionality of the resulting combined embedding, E_C , is compatible with the symmetric encoder-decoder U-Net architecture. The combined embedding, E_C , is then unflattened and fed only into the bottleneck of our U-Net decoder to produce the perceptually enhanced image, I_Y . *All-in-all, our EM offers a unique application-specific conditioning solution without requiring computationally demanding conditioning at every layer [18, 31] or a dedicated network for merging images and texts in the input [42] or enlarged decoder capacity due to size mismatch originated from concatenating text and image embeddings at the bottleneck [11, 38].* The architecture of our perceptual translation module, G , and our strategy for guiding the model with text prompts are illustrated in Fig. 2. Detailed architectural configurations of our MLP and the pre-trained CLIP model are available in the supplementary’s Sec. 2.3.

Sample size adaptive loss. When introducing new tasks in the training of G , the number of samples available for a new task may be limited compared to the existing tasks. Thus, we introduce a sample count adaptive loss function that regularizes G in training according to the number of samples available for each task. Considering the largest sample count among all tasks, SC_{MAX} , and the sample counts for each task, SC_T , we calculate boosting factors, B_T , inversely proportional to the sample counts, capped by a maximum boost coefficient, B_{MAX} . These boosting factors are then used to scale the L1 loss for each task,

$$B_T = 1 + (B_{MAX}(1 - \frac{SC_T}{SC_{MAX}})) \quad (1)$$

$$\mathcal{L}_{taL1} = \mathcal{L}_{L1}(I_Y, I_{GT})B_T.$$

By amplifying the loss inversely proportional to the sample counts for tasks with fewer samples, we ensure optimal use of available data for each task and encourage the optimization process to allocate greater updates to the model parameters corresponding to these underrepresented tasks. We further evaluate sample size adaptive L1 loss in our ablation study in Sec. 4.

Task-aware discriminator component. It has been demonstrated that utilizing conditional GAN loss [16] effectively regularizes image translation tasks by improving the quality of generated images while preserving the original content. Building on the image-based conditioning proposed by Isola et al. [16], we extend this approach to include task conditioning in our adversarial loss. To guide the

training of our model, we employ a multitasking task-aware discriminator, D . This discriminator processes the generated image, I_Y , the input image, I_X , and the task-specific text embeddings, E_T , to generate probability maps that facilitates the calculation of the task-aware adversarial loss. To support this operation, the task embeddings, E_T , are stacked and concatenated along the channel dimension of the I_Y and I_X . The resulting tensor, which comprises both the image and task information, is subsequently fed into D to obtain a prediction map, P . Our multitasking task-aware discriminator is illustrated in Fig. 2. We leverage probability maps, P , which provide a pixel-wise estimation of the likelihood that each pixel belongs to the perceptually enhanced image, I_Y . These probability maps are generated by our multitasking task-aware discriminator, D , and are used to enhance task-aware guidance during the training of G as shown in the following equation:

$$P_0 = D(I_X, I_{GT}, E_T) \quad P_1 = D(I_X, I_Y, E_T) \quad (2)$$

$$\mathcal{L}_{tcGAN} = \mathbb{E}_{I_X, I_{GT}, E_T} [\log P_0] + \mathbb{E}_{I_X, I_Y, E_T} [\log(1 - P_1)].$$

Objective functions and training procedure. We guide the training of our model by utilizing the following functions: (1) a sample size adaptive L1 loss, and (2) a task-aware adversarial loss. Our total loss function is formulated as shown in Eq. (3), where λ is a hyperparameter that adjusts the contribution of the sample size adaptive loss to the total loss,

$$\mathcal{L}_{total} = \mathcal{L}_{tcGAN} + \lambda \mathcal{L}_{taL1}. \quad (3)$$

We use a two-phase training strategy. Initially, our training dataset is restricted to image pairs from single tasks, which allows the model to focus on learning each task independently. After completing this phase, we expand our training dataset by incorporating both single and combined task image pairs, and continue the training process. Hyperparameters and training details are available in the supplementary’s Sec. 2.6.

Embedding streaming component. Optionally, in scenarios where computational resources and bandwidth are extremely limited, streaming the generated images in a compressed form to the user can be beneficial for presenting high quality media. For such cases, our model can be deployed on a more powerful server, where the generated images are compressed and streamed to the client. To support this, we utilize a distilled version of the pre-trained encoder and decoder [34], where images are compressed using the encoder. The compressed images are then streamed to the client, where they are decompressed by the decoder to be displayed. This component is optional and can be disabled in scenarios where computational and bandwidth resources are not a concern. Practical details for our streaming component are available in the supplementary’s Sec. 2.4.

Perceptual graphics dataset. As our model learns a mapping from observed images, I_X , and text embeddings, E_T , to perceptually enhanced images, I_Y , denoted as $G : (I_X, E_T) \rightarrow I_Y$, it requires a dedicated set of image pairs for training. Generating paired image data can be challenging especially for more complex tasks such as chromostereopsis and the challenge can easily stack up as in our combined task cases. Thus, we propose a dataset containing 8800 image pairs, each with a resolution of 1024x1024 pixels, distributed equally

Table 2. Quantitative image quality analysis of our model in comparison to baseline models (vanilla U-Nets). The difference in performance is shown in parentheses indicating that our method is performing comparable to a single-task models even though multitasking. For the supported perceptual tasks, we use the following abbreviations: Foveation (F), Chromostereopsis (C), Image Denoising (ID), and Dynamic Range Enhancement (DRE).

Task	Model	PSNR (dB) \uparrow	SSIM \uparrow	LPIPS \downarrow	FovVideoVDP \uparrow
F	Single-task	27.43	0.79	0.18	9.23
	Ours	25.64 (-1.79)	0.74 (-0.05)	0.10 (+0.08)	9.01 (-0.22)
DRE	Single-task	33.38	0.92	0.05	9.25
	Ours	31.07 (-2.11)	0.88 (-0.04)	0.08 (-0.03)	9.06 (-0.19)
ID	Single-task	35.90	0.95	0.03	9.79
	Ours	34.05 (-1.85)	0.92 (-0.03)	0.08 (-0.05)	9.77 (-0.02)
C	Single-task	16.87	0.81	0.14	5.53
	Ours	17.04 (+0.17)	0.81 (0.00)	0.13 (+0.01)	5.54 (+0.01)
ID and C	Two-task	16.94	0.81	0.15	5.45
	Daisy-chain	16.02	0.73	0.16	5.43
DRE and C	Two-task	16.49	0.80	0.14	5.29
	Daisy-chain	16.27	0.80	0.14	5.27
ID and F	Two-task	15.91 (-0.58)	0.78 (-0.02)	0.16 (-0.02)	5.36 (+0.07)
	Ours	15.91 (-0.58)	0.78 (-0.02)	0.16 (-0.02)	5.36 (+0.07)
DRE and F	Two-task	27.15	0.78	0.22	9.16
	Daisy-chain	27.15	0.78	0.20	9.17
DRE and ID	Two-task	25.65 (-1.50)	0.71 (-0.07)	0.11 (+0.9)	8.98 (-0.19)
	Ours	25.65 (-1.50)	0.71 (-0.07)	0.11 (+0.9)	8.98 (-0.19)
F and C	Two-task	26.60	0.75	0.23	8.85
	Daisy-chain	26.59	0.76	0.21	8.84
DRE and ID and F and C	Four-task	25.06 (-1.54)	0.69 (-0.07)	0.11 (+0.10)	8.58 (-0.27)
	Ours	25.06 (-1.54)	0.69 (-0.07)	0.11 (+0.10)	8.58 (-0.27)
DRE and ID and F and C	Four-task	16.27	0.62	0.22	5.30
	Daisy-chain	12.46	0.30	0.36	4.06
DRE and ID and F and C	Ours	17.14 (+1.13)	0.66 (+0.04)	0.14 (+0.08)	5.61 (+0.31)
	Ours	17.14 (+1.13)	0.66 (+0.04)	0.14 (+0.08)	5.61 (+0.31)

across various perceptual tasks, including foveated rendering, dynamic range enhancement, image denoising, chromostereopsis, and their permutations. Our dataset is publicly available at [REVIEW].

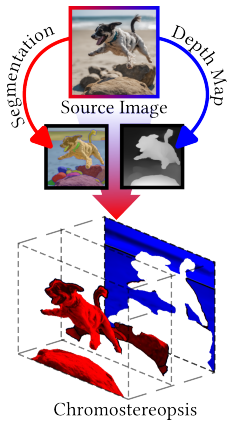


Fig. 3. We utilize depth [33] and segmentation [21] estimation to generate chromostereopsis images.

For the combined task image pairs, we apply the related methodology of each individual task consecutively. All supported tasks are listed in Tbl. 2, and details about the datasets can be found in the supplementary Sec. 3.

For all of our tasks, we generate RGB source images using Stable Diffusion [34]. Our foveated image examples rely on Walton et al. [39], for dynamic range enhancement we clip the dynamic range of the generated images from 8 bits to 4 bits, and for image denoising we add salt and pepper noise to the generated images. To induce the chromostereopsis effect, we first generate a depth map from the ground truth images using the monocular depth estimation method by Ranftl et al. [33], then segment these images following the method by Kirillov et al. [21]. The final chromostereopsis images are produced by adjusting the hue of the foreground segments to red and the background segments to blue, based on the average depth of each segment, as proposed by Westermann et al. [40]. A visualization of this process is shown in Fig. 3.

Table 3. Performance evaluation results of our multitasking perceptual model and baselines (vanilla U-Net) on desktop (NVIDIA RTX 3090) and embedded devices (NVIDIA Jetson Nano). We maintain a fair and even baseline boosting comparison by limiting model capacities to be equal per task (~ 7.6 M per task), while our model dedicates half the parameter count in its U-Net (~ 3 M) for all tasks, and dedicate rest of the parameters to Embedding Mapper component, *EM*, with feature sizes as small as U-Net’s bottleneck. Our model with a single inference step offers a fast solution suitable for desktop and embedded development.

Device	Model	Inference Speed (ms)	Parameter Count (M)	Task Count
Desktop	Single-task	1.34 ms	7.656 M	1
	Daisy-chain	3.79 ms	15.312 M	2
	Daisy-chain	7.65 ms	30.624 M	4
	Two-task	1.34 ms	7.656 M	2
	Four-task	1.34 ms	7.656 M	4
	Ours	1.74 ms	50.593 M	1-4
Embedded	Single-task	129.56 ms	7.656 M	1
	Daisy-chain	409.16 ms	15.312 M	2
	Daisy-chain	810.28 ms	30.624 M	4
	Two-task	129.56 ms	7.656 M	2
	Four-task	129.56 ms	7.656 M	4
	Streaming Component	179.14 ms	1.222 M	1-4
	Ours	260.82 ms	50.593 M	1-4

4 EVALUATION

We evaluate our learned model in terms of image quality (see Tbl. 2) and inference speed (see Tbl. 3). To assess image quality, we employ metrics such as Peak Signal-to-Noise-Ratio (PSNR), Structural Similarity Index Measure (SSIM), Learned Perceptual Image Patch Similarity Metric (LPIPS) [45], and FovVideoVDP [26]. We conduct a user study to further confirm the image quality produced by our model is comparable to the state-of-the-art methods. We include ablation studies for the sample size adaptive loss and task aware adversarial loss to investigate their impact. For more visual results beyond Fig. 10 and Fig. 11, consult our supplementary’s Sec. 4.

Inference speed. We compare our model’s performance against relevant baseline models to assess its image quality and inference speed. As there are no direct competitors in the literature to our proposed method, we formulate our baseline, which consists of vanilla U-Net models trained on our dataset and deployed in three different settings. These deployment settings are single-task, daisy-chain, and N-task, where N represents the number of simultaneously applied tasks. Here, a

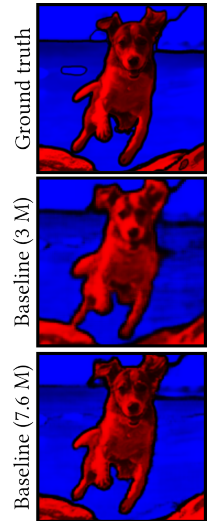


Fig. 4. Dedicating lower capacity than 7.6 million parameters per task leads to visual distortions in our baseline models.

single-task model refers to a model trained for a specific task (e.g., foveation); a daisy-chain model refers to running single-task models consecutively (e.g., image denoising and foveation); and an N-task model refers to a model trained with a specific combination of tasks to perform all tasks in a single inference.

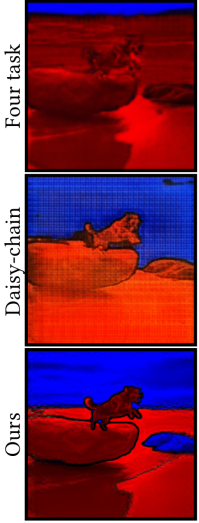


Fig. 5. Sample images with four perceptual tasks applied on various baseline models and ours.

For fair comparison, we set the model capacity of all models to be equal per task (i.e. ~ 7.6 million parameters per task) as reported in Tbl. 3. Although our model has ~ 50 million parameters excluding D ; the parameters for the U-Net for our model consumes only ~ 3 million parameters, which is half the size of other baseline models with ~ 7.6 million parameters dedicated to the U-Net at minimum. The remaining ~ 47 million parameters are used for the Embedding Mapper module (EM), where the feature sizes are close to bottleneck feature size in our U-Net. *Dedicating more parameters to the EM with small feature sizes help us to achieve inference speeds as fast as a single-task model while supporting all the benefits of text-guidance and multitasking with a single model.* If the baseline models use lower capacity in their U-Net following our model (~ 3 million parameters), they render visually distorted blurry images as sampled in Fig. 4, making these lower capacity baseline models unusable for comparison. We provide details for the lower capacity U-Net option in our supplementary’s Sec. 2. The baseline settings (single-task, daisy-chain, and N-task) are also limited in how many tasks they can support and do not offer any flexibility to blend tasks at will –lightly foveate and fully denoise is not an option for a foveation and denoising baseline–. This necessitates the training of many models for many tasks, making practical model management an issue especially for embedded devices. In comparison to the single-task and two-task models, Tbl. 3 shows that our model has similar inference speeds. Daisy-chain models are naturally slower than our model in inference speed due to dedicating larger capacities. Our model, as observed in Tbl. 3, offers inference speeds suitable for real time applications on both desktop and embedded devices.

Quantitative image quality. We evaluate the visual quality of our model and the baselines with established metrics in Tbl. 2 and provide sample visuals in Fig. 10 and Fig. 11 to understand their task performance qualitatively. We report the metrics in Tbl. 2 as an average over the test split of our dataset. Across various metrics, our models achieves image qualities comparable to our baselines while uniquely offering multitasking with half the parameter count in its U-Net portion. In addition to applying perceptual effects, our model also supports these effects at different intensities using adjectives in text-guidance such as “strongly foveate” as sampled in Fig. 10 and

Fig. 11. For additional visuals of other supported tasks, consult our supplementary’s Sec. 4.

Supporting complex tasks. Our model supports up to four tasks in a single inference step, with the ability to control the intensity of the applied effects. As indicated in the last row of Tbl. 2 and in Fig. 5, when the task count increases to four, our model surpasses both the daisy-chain method and the four-task models across all measured metrics. As the complexity of the combined tasks increases, the ability of the four-task model becomes insufficient for generating high-quality images. In contrast, our multitasking approach provides a flexible solution, allowing for the blending of tasks and the generation of high-quality images using a single model.

Ablation study. We conduct ablation studies to validate the effectiveness of our proposed components. Specifically, we evaluate the performance contribution of each component of our loss function. Additionally, we demonstrate the potential expansion of our model to support additional tasks. **Task-aware adversarial loss** Fig. 6 presents a representative sample image that demonstrates the impact of the task-aware adversarial loss. When we include the task-aware adversarial loss in our model, we observe that the model preserves high-frequency

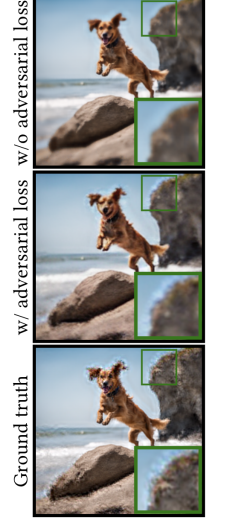


Fig. 6. Our task-aware adversarial loss helps our model to preserve feature at the periphery in Foveated rendering.

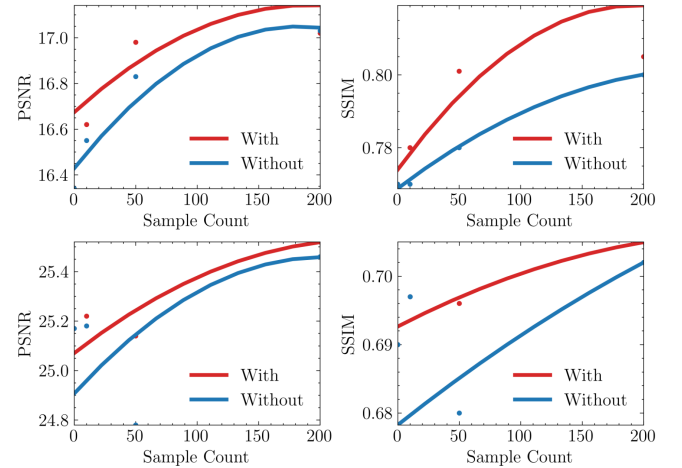


Fig. 7. Performance of our model in terms of PSNR and SSIM across various training sample sizes for two reduced tasks: image denoising and chromostereopsis (top row) and denoise and foveate (bottom row). Our model’s performance improves in low sample count scenarios when sample size adaptive loss is used. The plotted curves are second-degree polynomials fitted to the data.

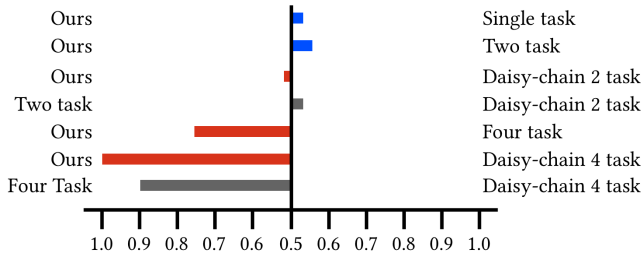


Fig. 8. Preferences of participants in the user study. Our model is on-par with single-task models, two-task models, and daisy-chaining of two models, while outperforming the daisy-chaining of four tasks and the four-task model in terms of user preference.

details of the image. Without the task-aware adversarial loss, the model fails to preserve these details similar to the baseline models. We invite readers to observe the high-frequency details in the foveated regions of the images in Fig. 6. **Sample size adaptive loss** to assess the performance on tasks with varying sample sizes of our method, we conduct additional evaluations. First, in our training dataset we reduced the sample count of a set of tasks to simulate a low sample count scenario. The reduced sample sizes are as follows: 0, 50, 100, 150, and 200, whereas a non-reduced task contain 880 samples. We measure performance using PSNR and SSIM, as shown in Fig. 7. The sample size adaptive loss improves the performance of our method on tasks with low sample counts.

Subjective evaluation. We conduct an informal subjective experiment to assess preferences between our model and the baselines, as shown in Fig. 8. Our study involved 22 participants (5 female, 17 male, aged 18-30) with normal or corrected-to-normal vision. The participants were naïve to the study’s objectives. Prior to the experiment, they were instructed to position themselves 50 cm away from the screen. The study consisted of five sections, each evaluating different tasks with 15 pairs of images. Before each section, participants were informed about the task and asked to rate the image pairs based on their preferences. The first four sections evaluated single tasks, while the last focused on combined tasks. Participants’ preferences indicate that our model performs on par with single-task models, two-task models, and the daisy-chaining of two models, with half of the participants preferring our model. For the four task cases, participants preferred our model with probabilities of 100% and 74% compared to the daisy-chaining of four tasks and the four-task model, respectively. The participants’ preferences are consistent with our quantitative results in Tbl. 2 and further support our findings about complex tasks in Sec. 4.

5 DISCUSSION

Our learned multitasking perceptual graphics model offers a flexible model that could be tailored to immersive displays’ needs with text-guidance. There are various limitations and potential future research directions that may help overcome these limitations.

Visual artifacts when using adjectives. Our model is trained using image pairs and their corresponding text prompts found in our

dataset. These text prompts and image pairs also contain adjectives such as “strongly,” “lightly,” or “mildly” in various training cases. In some test cases with these adjectives, we observe color deviations and a minor noise from the ground truth images as sampled in Fig. 9. In cases where we do not use adjectives, we do not observe such visual artifacts.

Supporting more tasks. Our model supports a fixed set of perceptual graphics tasks with their permutations in a single inference step. Adding more tasks involves expanding the dataset and training the model with these new tasks, provided that the model has sufficient capacity to learn them. Beyond the perceptual tasks demonstrated in our results at Fig. 10 and Fig. 11, there could be other perceptual graphics tasks that could be beneficial to support in the future. Namely, generating a stereo image pair from a single image source is one of these tasks. In addition, there are color based perceptual tasks that could help deliver power savings [12], prescription correction [13], anaglyph rendering [41], and accommodative rendering [8] in immersive display applications.

Task-specific visual quality metrics. Generic image quality metrics such as PSNR, SSIM, LPIPS and FovVideoVDP are not well suited for chromostereopsis and foveation cases, as shown in the first and third rows of Fig. 10. In the case of foveation, these metrics fail to capture the metameric patterns in the peripheral regions, which are essential for the task. In the case of chromostereopsis, they do not detect some artifacts that are present. This limitation restricts the ability to further improve the quality of the generated images through learned methods, such as super-resolution in our case. The findings of our practical super-resolution experiments using a pretrained model proposed by Lim et al. [24] are available in the supplementary’s Sec. 2.5.

Generalizing to unseen prompts. Our model supports a predefined set of prompts and their permutations. A potential research direction is to derive an improved version of our model supporting unseen prompts similar to the zero-shot capabilities of generative models for 3D scenes [25] or video [5].

Our new learned perceptual graphics model efficiently enhances images for immersive display applications, particularly targeting computationally limited platforms like VR headsets or AR glasses. The key finding from our model is effectively combining encoded RGB images and embeddings from text prompts for various perceptual tasks via multitask learning without exhausting computational resources. This finding enabled our model and help us guide perceptual graphics using both input images and text prompts. Our work encourages further research that could lead to more efficient methods supporting perceptual graphics on emerging mobile VR and AR platforms.

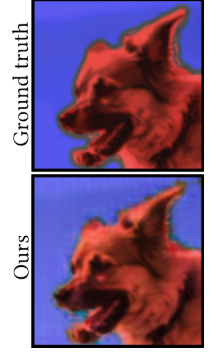


Fig. 9. Our model may generate visual artifacts when using adjectives such as “mildly.”

REFERENCES

- [1] Mahmoud Afffi and Michael S Brown. 2020. Deep white-balance editing. In *Proceedings of the IEEE/CVF Conference on computer vision and pattern recognition*. 1397–1406.
- [2] Yuejin Bai, Yana Zhang, and Zhaohui Li. 2016. Perceived depth modeling based on chromostereopsis. In *2016 2nd IEEE International Conference on Computer and Communications (ICCC)*. IEEE, 723–727.
- [3] Tim Brooks, Aleksander Holynski, and Alexei A Efros. 2023. Instructpix2pix: Learning to follow image editing instructions. In *Proceedings of the IEEE/CVF Conference on Computer Vision and Pattern Recognition*. 18392–18402.
- [4] Rich Caruana. 1997. Multitask learning. *Machine learning* 28 (1997), 41–75.
- [5] Duygu Ceylan, Chun-Hao P Huang, and Niloy J Mitra. 2023. Pix2video: Video editing using image diffusion. In *Proceedings of the IEEE/CVF International Conference on Computer Vision*. 23206–23217.
- [6] Jinyoung Choi and Bohyung Han. 2020. Task-aware quantization network for jpeg image compression. In *Computer Vision—ECCV 2020: 16th European Conference, Glasgow, UK, August 23–28, 2020, Proceedings, Part XX 16*. Springer, 309–324.
- [7] Yunjey Choi, Minje Choi, Munyoung Kim, Jung-Woo Ha, Sunghun Kim, and Jaegul Choo. 2018. StarGAN: Unified Generative Adversarial Networks for Multi-Domain Image-to-Image Translation. In *Proceedings of the IEEE Conference on Computer Vision and Pattern Recognition (CVPR)*.
- [8] Steven A Cholewiak, Gordon D Love, Pratul P Srinivasan, Ren Ng, and Martin S Banks. 2017. Chromablur: Rendering chromatic eye aberration improves accommodation and realism. *ACM Transactions on Graphics (TOG)* 36, 6 (2017), 1–12.
- [9] Marcos V Conde, Florin Vasluianu, Javier Vazquez-Corral, and Radu Timofte. 2023. Perceptual image enhancement for smartphone real-time applications. In *Proceedings of the IEEE/CVF Winter Conference on Applications of Computer Vision*. 1848–1858.
- [10] Arturo Deza, Aditya Jonnalagadda, and Miguel Eckstein. 2017. Towards metamerism via foveated style transfer. *arXiv preprint arXiv:1705.10041* (2017).
- [11] Hao Dong, Simiao Yu, Chao Wu, and Yike Guo. 2017. Semantic image synthesis via adversarial learning. In *Proceedings of the IEEE international conference on computer vision*. 5706–5714.
- [12] Budmonde Duinkharjav, Kenneth Chen, Abhishek Tyagi, Jiayi He, Yuhao Zhu, and Qi Sun. 2022. Color-perception-guided display power reduction for virtual reality. *ACM Transactions on Graphics (TOG)* 41, 6 (2022), 1–16.
- [13] Ahmet H Güzel, Jeanne Beyazian, Praneeth Chakravarthula, and Kaan Aksit. 2023. ChromaCorrect: prescription correction in virtual reality headsets through perceptual guidance. *Biomedical Optics Express* 14, 5 (2023), 2166–2180.
- [14] Ji Young Hong, Ho Young Lee, Du Sik Park, and Chang Yeong Kim. 2011. Depth perception enhancement based on chromostereopsis. In *Human Vision and Electronic Imaging XVI*, Vol. 7865. SPIE, 367–376.
- [15] Lianghua Huang, Di Chen, Yu Liu, Yujun Shen, Deli Zhao, and Jingren Zhou. 2023. Composer: Creative and controllable image synthesis with composable conditions. *arXiv preprint arXiv:2302.09778* (2023).
- [16] Phillip Isola, Jun-Yan Zhu, Tinghui Zhou, and Alexei A Efros. 2017. Image-to-image translation with conditional adversarial networks. In *Proceedings of the IEEE conference on computer vision and pattern recognition*. 1125–1134.
- [17] Seung-Won Jung and Sung-Jea Ko. 2012. Depth map based image enhancement using color stereopsis. *IEEE Signal Processing Letters* 19, 5 (2012), 303–306.
- [18] Tero Karras, Samuli Laine, and Timo Aila. 2019. A style-based generator architecture for generative adversarial networks. In *Proceedings of the IEEE/CVF conference on computer vision and pattern recognition*. 4401–4410.
- [19] Zhanghan Ke, Yuhao Liu, Lei Zhu, Nanxuan Zhao, and Rynson WH Lau. 2023. Neural preset for color style transfer. In *Proceedings of the IEEE/CVF Conference on Computer Vision and Pattern Recognition*. 14173–14182.
- [20] Jonghyun Kim, Youngmo Jeong, Michael Stengel, Kaan Aksit, Rachel A Albert, Ben Boudaoud, Trey Greer, Joohwan Kim, Ward Lopes, Zander Majercik, et al. 2019. Foveated AR: dynamically-foveated augmented reality display. *ACM Trans. Graph.* 38, 4 (2019), 99–1.
- [21] Alexander Kirillov, Eric Mintun, Nikhila Ravi, Hanzi Mao, Chloe Rolland, Laura Gustafson, Tete Xiao, Spencer Whitehead, Alexander C Berg, Wan-Yen Lo, et al. 2023. Segment anything. *arXiv preprint arXiv:2304.02643* (2023).
- [22] Kanghyeok Ko, Taesun Yeom, and Minhyeok Lee. 2023. Superstargan: Generative adversarial networks for image-to-image translation in large-scale domains. *Neural Networks* 162 (2023), 330–339.
- [23] George Alex Koulis, Kaan Aksit, Michael Stengel, Rafal K Mantiuk, Katerina Mania, and Christian Richardt. 2019. Near-eye display and tracking technologies for virtual and augmented reality. In *Computer Graphics Forum*, Vol. 38. Wiley Online Library, 493–519.
- [24] Bee Lim, Sanghyun Son, Heewon Kim, Seungjun Nah, and Kyoung Mu Lee. 2017. Enhanced deep residual networks for single image super-resolution. In *Proceedings of the IEEE conference on computer vision and pattern recognition workshops*. 136–144.
- [25] Chen-Hsuan Lin, Jun Gao, Luming Tang, Towaki Takikawa, Xiaohui Zeng, Xun Huang, Karsten Kreis, Sanja Fidler, Ming-Yu Liu, and Tsung-Yi Lin. 2023. Magic3d: High-resolution text-to-3d content creation. In *Proceedings of the IEEE/CVF Conference on Computer Vision and Pattern Recognition*. 300–309.
- [26] Rafal K Mantiuk, Gyorgy Denes, Alexandre Chapiro, Anton Kaplanyan, Gizem Rufo, Romain Bachy, Trisha Lian, and Anjul Patney. 2021. Fovvideovp: A visible difference predictor for wide field-of-view video. *ACM Transactions on Graphics (TOG)* 40, 4 (2021), 1–19.
- [27] Ismail Marzuki and Donggyu Sim. 2020. Perceptual adaptive quantization parameter selection using deep convolutional features for HEVC encoder. *IEEE Access* 8 (2020), 37052–37065.
- [28] Xiaoxu Meng, Ruofei Du, Matthias Zwicker, and Amitabh Varshney. 2018. Kernel Foveated Rendering. *Proc. ACM Comput. Graph. Interact. Tech.* 1, 1, Article 5 (jul 2018), 20 pages. <https://doi.org/10.1145/3203199>
- [29] Guy Ohayon, Theo Adrai, Gregory Vaksman, Michael Elad, and Peyman Milanfar. 2021. High perceptual quality image denoising with a posterior sampling cgan. In *Proceedings of the IEEE/CVF International Conference on Computer Vision*. 1805–1813.
- [30] Maris Ozolinsh and Kristine Muizniece. 2015. Color Difference Threshold of Chromostereopsis Induced by Flat Display Emission. *Frontiers in Psychology* 6 (2015). <https://doi.org/10.3389/fpsyg.2015.00337>
- [31] Or Patashnik, Zongze Wu, Eli Shechtman, Daniel Cohen-Or, and Dani Lischinski. 2021. Styleclip: Text-driven manipulation of stylegan imagery. In *Proceedings of the IEEE/CVF international conference on computer vision*. 2085–2094.
- [32] Alec Radford, Jong Wook Kim, Chris Hallacy, Aditya Ramesh, Gabriel Goh, Sandhini Agarwal, Girish Sastry, Amanda Askell, Pamela Mishkin, Jack Clark, et al. 2021. Learning transferable visual models from natural language supervision. In *International conference on machine learning*. PMLR, 8748–8763.
- [33] René Ranftl, Alexey Bochkovskiy, and Vladlen Koltun. 2021. Vision transformers for dense prediction. In *Proceedings of the IEEE/CVF international conference on computer vision*. 12179–12188.
- [34] Robin Rombach, Andreas Blattmann, Dominik Lorenz, Patrick Esser, and Björn Ommer. 2022. High-resolution image synthesis with latent diffusion models. In *Proceedings of the IEEE/CVF conference on computer vision and pattern recognition*. 10684–10695.
- [35] Guolei Sun, Thomas Probst, Danda Pani Paudel, Nikola Popović, Menelaos Kanakis, Jagruti Patel, Dengxin Dai, and Luc Van Gool. 2021. Task switching network for multi-task learning. In *Proceedings of the IEEE/CVF international conference on computer vision*. 8291–8300.
- [36] Ximeng Sun, Rameswar Panda, Rogerio Feris, and Kate Saenko. 2020. Adashare: Learning what to share for efficient deep multi-task learning. *Advances in Neural Information Processing Systems* 33 (2020), 8728–8740.
- [37] Taimoor Tariq and Piotr Didyk. 2024. Towards Motion Metamers for Foveated Rendering. *ACM Trans. Graph.* (2024).
- [38] Duc Minh Vo and Akihiro Sugimoto. 2022. Paired-D++ GAN for image manipulation with text. *Machine Vision and Applications* 33, 3 (2022), 45.
- [39] David R Walton, Rafael Kuffner Dos Anjos, Sebastian Friston, David Swapp, Kaan Aksit, Anthony Steed, and Tobias Ritschel. 2021. Beyond blur: Real-time ventral metamers for foveated rendering. *ACM Transactions on Graphics* 40, 4 (2021), 1–14.
- [40] Helena Westermann. 2022. Using Chromostereopsis to Enhance Depth Perception in Photos by changing the Hue. (2022).
- [41] Andrew J Woods and Chris R Harris. 2010. Comparing levels of crosstalk with red/cyan, blue/yellow, and green/magenta anaglyph 3D glasses. In *Stereoscopic displays and applications XXI*, Vol. 7524. SPIE, 235–246.
- [42] Weihao Xia, Yujiu Yang, Jing-Hao Xue, and Baoyuan Wu. 2021. Tedigan: Text-guided diverse face image generation and manipulation. In *Proceedings of the IEEE/CVF conference on computer vision and pattern recognition*. 2256–2265.
- [43] Haibao Yu, Tuopu Wen, Guangliang Cheng, Jiankai Sun, Qi Han, and Jianping Shi. 2020. Low-bit quantization needs good distribution. In *Proceedings of the IEEE/CVF Conference on Computer Vision and Pattern Recognition Workshops*. 680–681.
- [44] Kai Zhang, Wangmeng Zuo, Yunjin Chen, Deyu Meng, and Lei Zhang. 2017. Beyond a gaussian denoiser: Residual learning of deep cnn for image denoising. *IEEE transactions on image processing* 26, 7 (2017), 3142–3155.
- [45] Richard Zhang, Phillip Isola, Alexei A Efros, Eli Shechtman, and Oliver Wang. 2018. The unreasonable effectiveness of deep features as a perceptual metric. In *Proceedings of the IEEE conference on computer vision and pattern recognition*. 586–595.
- [46] Jun-Yan Zhu, Taesung Park, Phillip Isola, and Alexei A Efros. 2017. Unpaired image-to-image translation using cycle-consistent adversarial networks. In *Proceedings of the IEEE international conference on computer vision*. 2223–2232.

Received 20 February 2024; revised 20 February 2024; accepted 20 February 2024

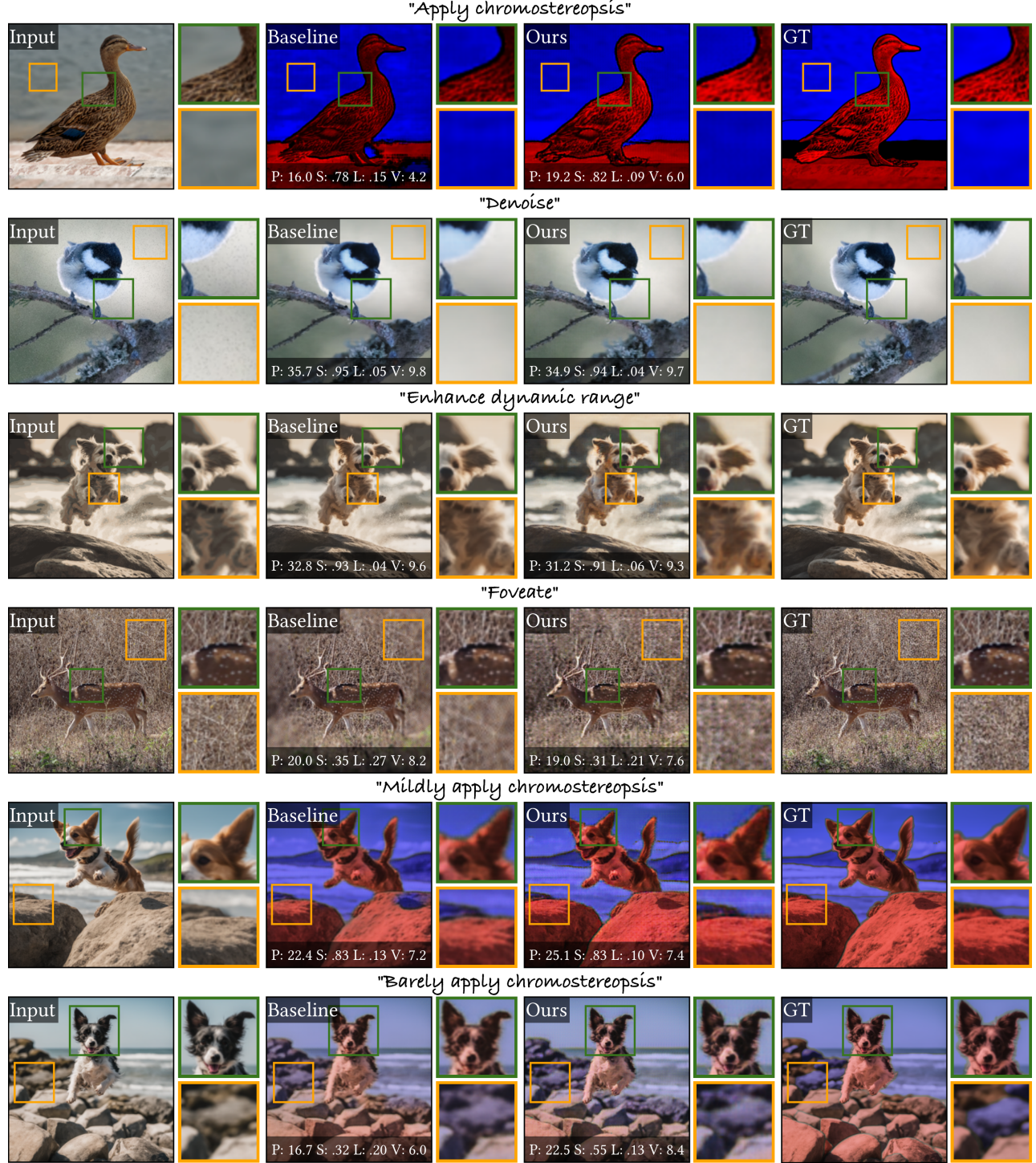


Fig. 10. Results of our proposed multitasking perceptual model (~ 50 M) compared to task specific trained Vanilla U-Nets (~ 7.6 M per task). Following abbreviations are used for metrics: PSNR (P) \uparrow SSIM (S) \uparrow LPIPS (L) \downarrow FovVideoVDP (V) \uparrow . (Sources of input images from rows 1, 2, and 4: Miguel Discart, Kuhnmi, and Lahar Jadav. The rest of the input images are generated using Stable Diffusion [34].)

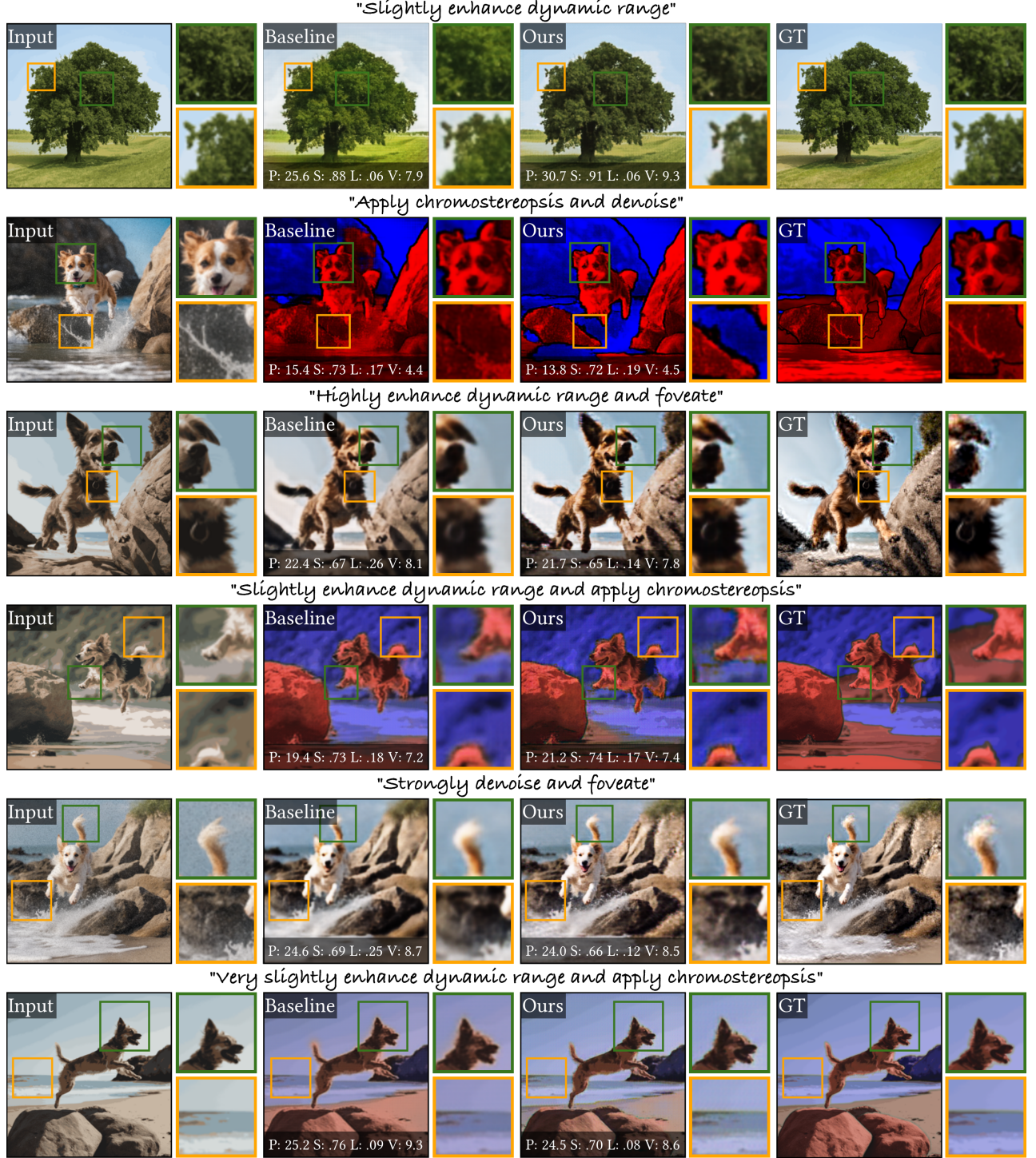


Fig. 11. Results of our proposed multitasking perceptual model (~ 50 M) compared to task specific trained Vanilla U-Nets (~ 7.6 M per task). Following abbreviations are used for metrics: PSNR (P) \uparrow SSIM (S) \uparrow LPIPS (L) \downarrow FovVideoVDP (V) \uparrow . (Source of input image from first row: Rainer Lippert. The rest of the input images are generated using Stable Diffusion [34].)